Image Restoration for Field Emission X-ray Source Array Based Radiographic Imaging

Kai Wang, Xi Chen, Haitao Cheng, Qinrong Qian and Xuanqin Mou

***Abstract*—Field emission x-ray source array is an emerging technology with some advantages compared with conventional x-ray source. In this work, a radiographic scheme based on field emission x-ray source array was proposed to study its possible application in radiation imaging. Each x-ray source in the array emits a cone beam x-ray through part of the object, and all the sources are overlapped to cover the whole object. Two x-ray source scan strategies, grouped scan strategy and simultaneous scan strategy, were studied. A projection rebinning based image restoration algorithm was introduced for the imaging schemes. Numerical simulations demonstrated that both scan strategies were effective for image restoration. Specifically, the grouped scan strategy produced fewer artifacts than the simultaneous scan strategy due to the non-overlap projections, while the simultaneous scan strategy enables faster imaging considering the inherent simultaneous data collection mode. This feasibility study illustrated that the field emission x-ray source array based radiographic scheme may offer a promising image modality.**

***Index Terms*—Radiography, field emission x-ray source array, image restoration, projection rebinning.**

I. Introduction

In recent years, x-ray sources with field emission cathodes have been developed [1]. Compared with the conventional thermionic systems, field emission sources have some advantages, such as high temporal resolution, smaller focal spots and programmable x-ray radiation [1-4]. Besides, the field emission based x-ray sources showed the potential for miniaturization and creating dense arrays of discrete and individually controlled x-ray sources, this further makes the design of new imaging geometries more flexible [2-4].

Chen et al. developed a 2D x-ray source array using ZnO nanowire field emitters which could achieve uniform distribution of x-ray generation [2], the schematic diagram of the flat-panel X-ray source is illustrated in Fig. 1. ZnO nanowires as field emission cathodes, are uniformly distributed and have similar morphologies, uniform electrons emit from the ZnO nanowires and strike the tungsten film, then generate x-rays with a small divergence angle.

In traditional x-ray radiography, x-ray tube emits radiation from a single focal spot, because of the limited cone beam angle, an appropriate distance between single point x-ray source and object is required, which make it difficult to reduce the system size, and may expose the patient and operator to unnecessary radiation [5]. Additionally, a diverging x-ray cone beam leads to image distortion of the objects due to inherent geometric magnification.

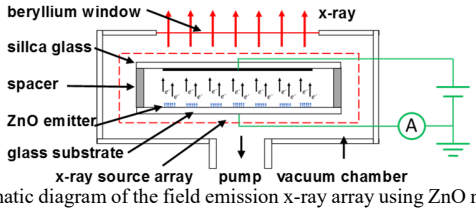

Fig. 1 Schematic diagram of the field emission x-ray array using ZnO nanowire field emitters.

X-ray source array based on addressable field emission cathodes could be a solution. Each x-ray source of the field emission x-ray source array can be independently controlled, and emits small cone beam x-ray through a certain portion of the object. And series of x-ray source bins co-treat the area to detected to form an overlay, hence only the region of interest (ROI) is irradiated, and the radiation dose to the patient could be decreased. Combining the high temporal resolution and smaller focal spots properties of field emission x-ray source, a high quality radiographic image can be obtained at low dose level. Also, using a dense x-ray source array, ROI could be irradiated with less source-to-object distance, in this way, an x-ray imaging system with small size is possible.

Due to the special geometry, projection image formation using field emission x-ray source array can conceptually take two forms: sequential exposure from non-overlapping source bins, or flash all the x-ray source bins simultaneously and get an overlapped projection image. Compare to the traditional radiography, which provides internal structure information of the whole area to be detected in one image, neither of the two forms could provide intuitive data for diagnostics or evaluation. Therefore, corresponding projection image restoration processing is necessary.

To study the application of the proposed 2D field emission x-ray source array in radiation imaging [2], and make full use of the properties of field emission x-ray tubes, in this work, we propose a radiographic scheme based on 2D field emission x-ray source array. Corresponding to the geometry, two ways of x-ray projection strategies, and a projection image restoration algorithm based on projection rebinning is proposed. Numerical simulations were performed to verify the effectiveness of the proposed approach.

II. Methods and Materials

A. System description

A radiographic scheme based on 2D field emission x-ray source array is proposed, shown as Fig. 2 and Fig. 3(a). Uniform field emission x-ray source bins are used and evenly placed in the same plane to form the 2D source array, consistent with the

This work was supported in part by the National Key Research and Development Program of China (No. 2016YFA0202003) and the National Natural Science Foundation of China (No. 61401349, No. 61571359).

The authors are with the Institute of Image Processing and Pattern Recognition, Xi'an Jiaotong University, Xi'an, Shaanxi 710049, China.

DOI: 10.12059/Fully3D.2017-11-3203018

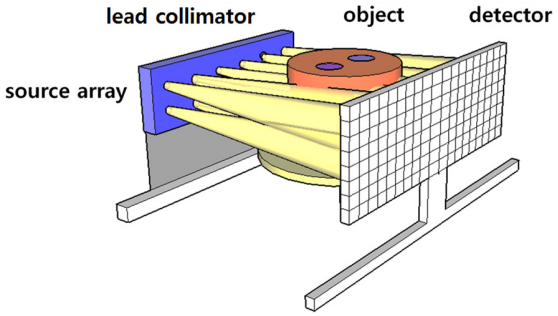

Fig. 2. Schematic diagram of the radiographic system using field emission x-ray source array. Uniform sources are evenly placed in a plane to form the 2D source array, each source emits cone beams which go through a portion of the area to be detected, and all the sources co-treat the detection area to form an overlay.

structure in [2]. A lead collimator with conical holes is placed in front of the source array to form cone beam x-rays with the same beam angle and direction. Every x-ray source bin emits cone beam x-ray through a certain portion of the area to be detected, and to obtain information of the object's internal structure, all the sources co-treat the whole object to form a seamless coverage. A flat panel detector is placed parallel to the plane of the 2D source array to collect the projection data.

B. *Forward Projection Model*

Corresponding to the proposed geometry, there are two ways of x-ray projection strategies. The first one is to divide the sources into different groups, each group consists of sources where the associated projection data have no overlap, and the system collects non-overlapping projection images by flashing the groups sequentially (referred as grouped projection hereafter). The other one is that all the x-ray sources flash simultaneously and get an overlapped projection image (referred as simultaneous projection hereafter).

In traditional radiography, x-rays emitted by the single x-ray source and travel through the objects, according to the Lambert-Beer law, the x-ray intensity detected by the detector bin $p(p = 1, \cdots, P)$ can be given as

$$I_p = I_{p0}\exp(-\sum_{n=1}^{N} a_{pn}x_n) + n_p \quad (1)$$

where I_{p0} is the photon number emitted from the source to the detector bin, N is the voxel number of the detected object, a_{pn} is the length at which the ray-path intersects voxel n, x_n is the attenuation coefficient of voxel n, n_p is the random noise.

When flashing the source groups sequentially, the projection data do not overlap, the detected x-ray intensity can still be modelled as Eq. (1), and given by

$$y_{pq} = \bar{y}_{pq} + n_{pq} \quad (2)$$

where $\bar{y}_{pq} = \sum_{n=1}^{N} a_{pqn}x_n$ is the integral of attenuation coefficient (referred as ray-sum hereafter) on the ray path pq, and y_{pq} is the detected ray-sum with random noise.

When flashing the total sources simultaneously, Eq. (1) can be modified as

$$I_p = \sum_{q=1}^{Q} I_{pq0}\exp(-\sum_{n=1}^{N} a_{pn}x_n) + n_p \quad (3)$$

Compare to the traditional radiography, which provides internal structure information of the whole area to be detected in one image, neither of proposed strategies could provide intuitive data for diagnostics or evaluation. The first strategy provides series of clear and non-overlapping data, each of which represents a part of the object. The second strategy provides information in one image, but it is overlapped. To alleviate this problem, a projection image restoration algorithm based on projection rebinning is proposed.

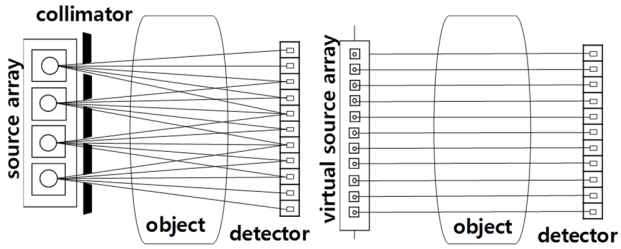

Fig. 3. Illustration of the projection image restoration problem. (a) The x-ray source array projection geometry, cone beam x-rays are emitted from every source. (b) The virtual source array projection geometry, parallel pencil beam x-rays are emitted form virtual source bins, travelling through the object, and detected by their corresponding detector bins.

C. *Image Restoration Algorithm*

To obtain a relatively clear restoration image for diagnostics or evaluation, a virtual parallel pencil beam projection model is assumed, and a restoration algorithm from x-ray source array projection to the parallel pencil beam projection is proposed.

Suppose that there is a virtual x-ray source plane which coincides with the position of the real x-ray source plane and has the same number of x-ray sources as the detector bins. Each virtual x-ray source emits parallel pencil beam x-rays with the same photon number I' travelling through the object, and the attenuation signal is detected by its corresponding detector bin without any scatter or quantum noise, shown as Fig. 3(b). The photon number detected by detector bin p in virtual projection can be modeled as

$$I'_{p'p} = I'\exp(-\sum_{n=1}^{N} b_{p'pn}x_n) \quad (4)$$

where p' is the corresponding virtual x-ray source of detector p, and $b_{p'pn}$ is the virtual beam length of the intersection with voxel n. The ray-sum on the ray path from the virtual source p' to the detector p can be modeled as

$$g_{p'p} = g_p = \sum_{n=1}^{N} b_{pn}x_n \quad (5)$$

where virtual path $p'p$ is simplified as path p because of the one-to-one relationship of virtual source p' and detector p.

Based on the introduced virtual projection, the sum of the attenuation coefficient on the virtual ray path p is represented by g_p, which is defined as the objective of the restoration problem. Through a linear transformation or a nonlinear method, $\bar{y}_{pq}$ can be approximately estimated with g_p [6]. A linear transformation matrix W is introduced to describe the relationship between $\bar{y}_{pq}$ and g_p, and is given by

$$\bar{y}_{pq} = \sum_{i=1}^{P} w_{pqi}g_i \quad (6)$$

where w_{pqi} is the element of W.

With the measurement and virtual projection models constructed, the objective function for image restoration can be established. The image restoration is performed by minimizing the cost function comprising a data term and regularization term. When using the grouped projection strategy, by substituting Eq. (2) into Eq. (6) the objective function for image restoration can be written as

$$\hat{g} = \arg\min_{g} ||Wg - y||_2^2 + \beta R(g) \quad (7)$$

where $g \in \mathbb{R}_+^P$ is the restoration image, $y \in \mathbb{R}_+^{PQ}$ is the measured noisy projection data, $R(g)$ is a (edge-preserving) regularization function and β balances the data-fit term and regularization term. When using the simultaneous projection strategy, considering Eqs. (3) and (6), the objective function for image restoration can be written as

$$\hat{g} = \arg\min_{g} \sum_{p=1}^{P} \left\| I_p - \sum_{q=1}^{Q} I_{pq} \exp\left(-w_{pq} g\right) \right\|^2 + \beta R(g) \quad (8)$$

D. A Simple Projection Rebinning Method

In order to simplify the calculation of the linear transformation matrix W, a simple but effective projection rebinning method is used [6], each oblique (cone beam) ray-sum is estimated form a single virtual pencil beam ray-sum which goes through the center point of the ray path in the object, as illustrated in Fig. 4. Define M as the mid-point of the intersection of the fan-line with the region of interest (ROI), d as the distance between the source plane and the detector plane, and $\|pq\|$ the distance between x-ray source q and detector p, corresponding oblique beam ray-sum can be approximately calculated as

$$\bar{y}_{pq} \approx \frac{\|pq\|}{d} g_i \quad (9)$$

where g_i is the selected virtual pencil beam ray-sum.

Considering a smaller cone angle of the field emission x-ray source, image restoration with better quality can be expected.

E. Experiments

To demonstrate the imaging efficacy of the proposed radiographic scheme with the projection image restoration algorithm, two simulation experiments on a simple cube phantom and a MOBY phantom were conducted [7]. As shown in Fig. 5. The cube phantom is a water cube, and four bone with different thickness were symmetrically inserted in. Dimension of the cube phantom is 50×256×256, and the MOBY phantom is 256×256×256, both of the phantoms are with a pixel size of $0.25\times0.25\times0.25\text{mm}^3$.

Two kinds of monochromatic projection strategies were analytic simulated with a fast-ray tracing technique [8]. And the dimension of the source array is 9×9, with a spacing of 5mm×5mm, every x-ray source in this array has a half cone beam angle of 5°. Due to the different size of the two phantoms, distances from the source plane to the center of object are 50mm and 121mm, and the distance from the source plane to the panel detector is 100mm and 172mm. A 360×360 panel detector with a bin size of $0.25\times0.25\text{mm}^2$ is applied to capture all the projection data.

With the measurement and projection models constructed, the radiographic image restoration is performed by minimizing the cost function (Eqs. (7) and (8)), in which the regularization term is chosen as total variation (TV) [9], and Nesterov's first order methods are employed to boost the algorithm [10].

III. Results

We present several projection images and image restoration results in Fig. 6, and quantitative evaluation using root mean square error (RMSE) in Table I. Projection images under the two scan strategies of the cube phantom and the MOBY phantom are used to demonstrate the feasibility of the radiographic system and evaluate the proposed image restoration algorithm.

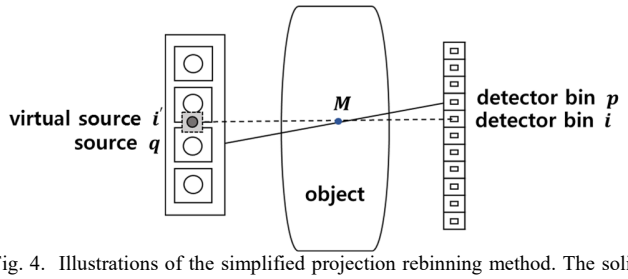

Fig. 4. Illustrations of the simplified projection rebinning method. The solid line is the ray path from source q to the detector bin p, and M is the mid-point of the intersection of the fan-line with the ROI, the dash line is the corresponding virtual x-ray, which is emitted from virtual source i' to detector bin i, and passes through M.

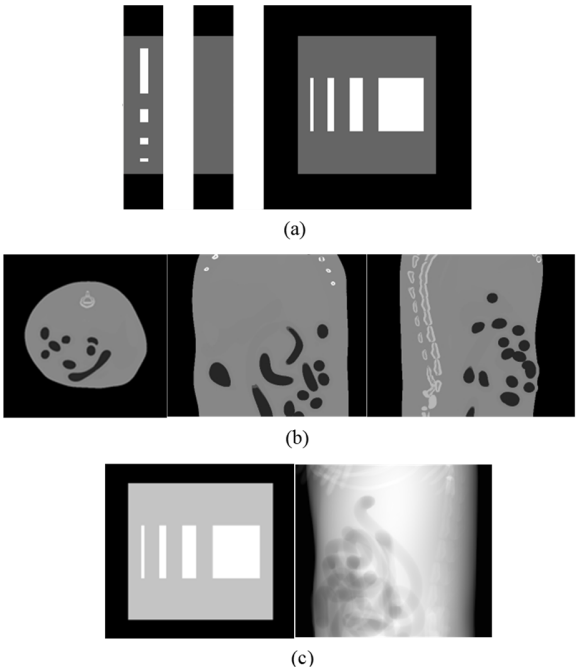

Fig. 5. Illustrations of the phantoms used in the simulations. (a) The central coronal (left), sagittal (middle), and transverse (right) views of the cube phantom. (b) The central coronal (left), sagittal (middle), and transverse (right) views of the MOBY phantom. (c) The ideal parallel pencil beam projection images of the cube phantom (left) and MOBY phantom (right).

One of the grouped projection images of the cube phantom is showed in Fig. 6(a), which is a projection of a portion of the object and has no overlap. The simultaneous projection image of the whole cube phantom is shown in Fig. 6(b), which contains the projection data form all the source array in one image but severely overlapped.

Image restoration result of the cube phantom is depicted in Fig. 6(c), where the restored images from grouped projection and simultaneous projection, and the difference between the restored projection images and the ideal projection image were illustrated. It is shown that, for both scanning strategies, the restoration results are clear in structure, and the RMSE are 0.0070cm^{-1} and 0.0074cm^{-1}. The result using grouped projection appears to be better, because of the uniform visual effects and less difference between the parallel pencil beam projection image. Residual errors occur mainly at the junction of different substances, due to the shape edges.

Result of the MOBY phantom, whose structure is relatively

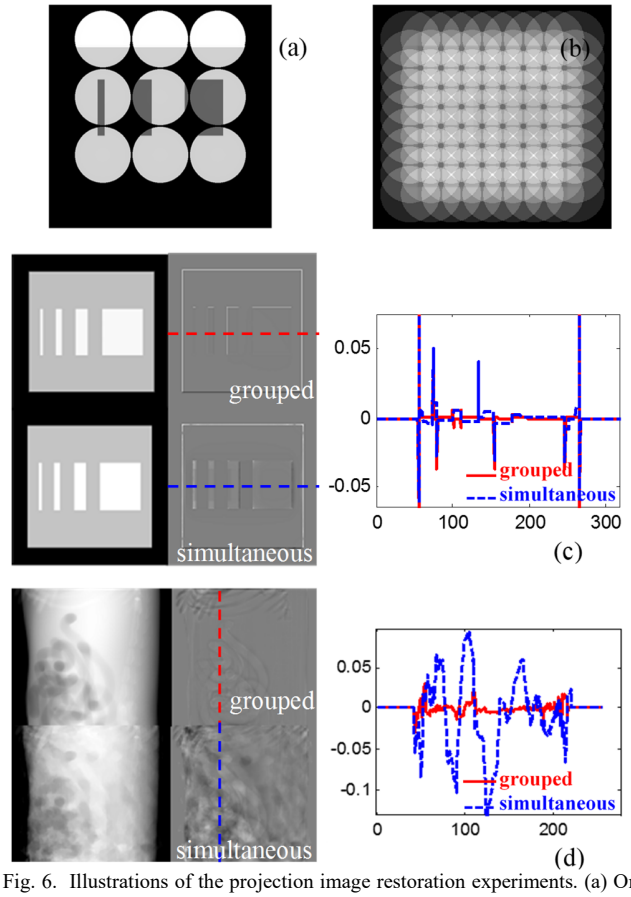

Fig. 6. Illustrations of the projection image restoration experiments. (a) One of the grouped projection images of the cube phantom, which is a projection of part of the object. (b) The simultaneous projection image of the whole cube phantom, which is severely overlapped. (c) The restoration results of the cube phantom, and the differences between the restored images and their corresponding parallel pencil beam projections. The profile is showed on the right. (d) The restoration result of the MOBY phantom, and the differences between the restored images and their corresponding parallel pencil beam projections. The profile is showed on the right.

complex and has a greater thickness, is depicted in Fig. 6(d). It is shown that, when using grouped projection, the restoration results appear to be clear in structure and the corresponding RMSE is small ($0.0158 cm^{-1}$); when using simultaneous projection, the contour of the phantom is well recovered, but internal structure is blurred, tissues and organs are difficult to distinguish, the corresponding RMSE is large ($0.0450 cm^{-1}$).

IV. Discussion

As a new technology, 2D source array with field emission x-ray tube was introduced to construct a radiographic imaging system, corresponding scan schemes and projection image restoration algorithm were proposed to predict the quality of this novel radiographic imaging method. Note that the x-ray source array based on field emission is not only tailored for radiography though we used the technology to construct a radiographic scheme in this work, it is expected that using the source array combined with the proposed scan strategies and projection restoration algorithm could also be applied to other radiation imaging systems, for example, CT and tomosynthesis, and a rotation free system might be expected.

Distance between adjacent x-ray source units, cone beam angle and distance from source plane to object are the key factors when designing the radiographic imaging system, and will directly affect the projection image restoration quality. The relationship between these parameters and the imaging quality will be investigated in the future.

As mentioned above, the projection rebinning method adopted here is simple but inexact, when detecting a complex phantom with simultaneous projection, it's difficult to obtain a clear restoration image. One of our future work will be to design a more accurate projection rebinning algorithm to improve the restoration quality.

Scatter is an important factor that influences the imaging quality. Future work will perform a Monte Carlo simulation to examine the effect of scatter in this system when using different scan strategies, and corresponding image restoration cost function will be re-established considering the statistical characteristics of the projection signal.

TABLE I
QUANTITATIVE EVALUATION OF THE PROJECTION IMAGE RESTORATION RESULTS IN TERM OF RMSE (UNIT cm^{-1})

Phantom	Grouped Projection	Simultaneous Projection
Cube	0.0070	0.0074
MOBY	0.0158	0.0450

V. Conclusion

We presented a radiographic scheme based on 2D field emission x-ray source array. We have shown that the geometry, combined with the proposed scan strategies and projection image restoration algorithm may offer a path for noninvasive imaging in biomedical research and industrial inspection. Promising image quality could be obtained using the grouped scan strategy, and a fast imaging speed could be achieved using the simultaneous scan strategy but with some blur.

References

[1] Sugie H, Tanemura M, Filip V, et al. Carbon nanotubes as electron source in an x-ray tube[J]. Applied Physics Letters, 2001, 78(17):2578-2580.
[2] Chen D, Song X, Zhang Z, et al. Transmission type flat-panel x-ray source using ZnO nanowire field emitters[J]. Applied Physics Letters, 2015, 107(24):243105.
[3] Grant E J, Posada C M, Castaño C H, et al. Electron field emission Particle-In-Cell (PIC) coupled with MCNPX simulation of a CNT-based flat-panel x-ray source[J]. Proceedings of SPIE - The International Society for Optical Engineering, 2011, 7961:796108-796108-11.
[4] Travish G. Addressable flat-panel x-ray sources for medical, security, and industrial applications[J]. Proceedings of SPIE - The International Society for Optical Engineering, 2012, 8502(7).
[5] Hendee W R, Ritenour E R, Hoffmann K R. Medical Imaging Physics, Fourth Edition[J]. Medical Physics, 2003, 30(4):730-730.
[6] Noo F, Defrise M R. Single-slice rebinning method for helical cone-beam CT.[J]. Physics in Medicine & Biology, 1999, 44(2):561-570.
[7] Segars W P, Tsui B M, Frey E C, et al. Development of a 4-D digital mouse phantom for molecular imaging research.[J]. Molecular Imaging & Biology Mib the Official Publication of the Academy of Molecular Imaging, 2004, 6(3):149-59.
[8] Siddon R L. Fast calculation of the exact radiological path for a three - dimensional CT array[J]. Medical Physics, 1985, 12(2):252-255.
[9] Sidky E Y, Kao C M, Pan X. Accurate image reconstruction from few-views and limited-angle data in divergent-beam CT[J]. Journal of X-ray science and technology, 2006, 14(2):119-139.
[10] Kim D, Ramani S, Fessler J A. Accelerating X-ray CT ordered subsets image reconstruction with Nesterov's first-order methods[C]//Proc. Intl. Mtg. on Fully 3D Image Recon. in Rad. and Nuc. Med. 2013: 22-5.